Preparation and Li Storage Properties of Hierarchical Porous Carbon Fibers Derived from Alginic Acid

ARTICLE *in* CHEMSUSCHEM · JUNE 2010

Impact Factor: 7.66 · DOI: 10.1002/cssc.201000035 · Source: PubMed

7 AUTHORS, INCLUDING:

Xing-Long Wu
Northeast Normal University
61 PUBLICATIONS **3,165** CITATIONS
SEE PROFILE

Sen Xin
Hefei University of Technology
43 PUBLICATIONS **1,789** CITATIONS
SEE PROFILE

Yu-Guo Guo
Chinese Academy of Sciences
170 PUBLICATIONS **10,860** CITATIONS
SEE PROFILE

DOI: 10.1002/cssc.201000035

Preparation and Li Storage Properties of Hierarchical Porous Carbon Fibers Derived from Alginic Acid

Xing-Long Wu,[a] Li-Li Chen ,[a, b] Sen Xin,[a] Ya-Xia Yin,[a] Yu-Guo Guo,*[a] Qing-Shan Kong,[b] and Yan-Zhi Xia[b]

One-dimensional (1D) hierarchical porous carbon fibers (HPCFs) have been prepared by controlled carbonization of alginic acid fibers and investigated with scanning electron microscopy (SEM), transmission electron microscopy (TEM), X-ray diffraction (XRD), X-ray photoelectron spectroscopy (XPS), Raman spectroscopy, nitrogen adsorption–desorption isotherms, and electrochemical tests toward lithium storage. The as-obtained HPCFs consist of a 3D network of nanosized carbon particles with diameters less than 10 nm and exhibit a hierarchical porous architecture composed of both micropores and mesopores. Electrochemical measurements show that HPCFs exhibit excellent rate capability and capacity retention compared with commercial graphite when employed as anode materials for lithium-ion batteries. At the discharge/charge rate of 45 C, the reversible capacity of HPCFs is still as high as 80 mA h g^{-1} even after 1500 cycles, which is about five times larger than that of commercial graphite anode. The much improved electrochemical performances could be attributed to the nanosized building blocks, the hierarchical porous structure, and the 1D morphology of HPCFs.

Introduction

As a renewable resource, biomass has become more and more attractive in the preparation of useful carbon materials,[1] especially hierarchical porous carbon materials (HPCMs). Biomass such as wood, coconut,[2] rice straw,[3] and starch[4] have been used to prepare porous activated carbons. With the fast development of ocean exploration, more and more attention has been paid to the utilization of abundant sea resources as the ocean occupies three-quarters of the earth's surface. Alginate, a natural polysaccharide extracted from marine brown algae, has attracted considerable attention ever since its discovery by Stanford in 1881. An important feature of alginate is the gelating behavior in the presence of divalent cations, which accounts for their extensive applications in immobilization of enzymes and proteins,[5] controlled delivery of drugs,[6] and wound management industry.[7] However, few studies have been reported concerning the preparation of carbon materials from alginates. Alginate has abundant carboxyl and hydroxyl groups in its polymeric carbon matrix. When all these functional groups have been converted to carbon oxides and water, the polymeric carbon matrix can be naturally converted to carbonaceous materials upon carbonization, making alginate a suitable precursor for the fabrication of porous carbon materials.

Due to the low cost, eco-friendliness, highly thermal and chemical stability as well as low electrochemical potential toward lithium insertion, carbonaceous materials have been widely studied as anode materials for rechargeable lithium-ion batteries (LIBs), which are generally considered to be one of the most state-of-the-art power devices for a variety of consumer and military applications.[8–12] Graphite, a carbonaceous material with the highest degree of graphitization, is an important anode material widely used in commercial LIBs at present.[13] However, poor rate performance makes it impractical to be employed as the anode material for high-energy and high-power LIBs, the critical enabling technology in hybrid electric vehicles (HEVs) and plug-in hybrid electric vehicles (PHEVs). To improve the high-rate capabilities toward lithium storage, tremendous efforts have been devoted to the exploration of new carbonaceous materials, and many materials have been reported, such as carbon nanotubes,[14] porous carbon,[15,16] carbon fibers,[17,18] and hard carbon spherules.[19] As one of the hierarchically nanostructured materials,[20,21] HPCMs have attracted much attention due to their outstanding structural advantages. The hierarchical pores and nanometer-sized pore walls may not only provide an effective pathway for Li^+-containing electrolyte but remarkably decrease the Li^+ diffusion distance and time in bulk carbon.[16]

So far, it has been reported that HPCMs can be prepared through templating technology with mesoporous silica[22] and zeolites[23] as hard templates, and polymer foams or microspheres as well as amphiphilic copolymers as soft templates.[24–26] However, this technology usually involves multistep processes and the removal of sacrificial templates, therefore is

[a] X.-L. Wu,[+] L.-L. Chen ,[+] S. Xin, Y.-X. Yin, Prof. Y.-G. Guo
Key Laboratory of Molecular Nanostructure and Nanotechnology
Beijing National Laboratory for Molecular Sciences (BNLMS)
Center for Molecular Sciences, Institute of Chemistry
Chinese Academy of Sciences (CAS)
Beijing 100190 (P.R. China)
Fax: (+86) 10-62557908
E-mail: ygguo@iccas.ac.cn

[b] L.-L. Chen ,[+] Dr. Q.-S. Kong, Prof. Y.-Z. Xia
Advanced Fibers & Modern Textile Cultivation Base for State Key Laboratory
Qingdao University, Qingdao 266071 (P.R. China)

[+] These authors contributed equally to this work

too complicated to be carried out. Over the past decades, various chemical and physical activating methods have been developed, in which additional inorganic compounds are used as activating agents.[27,28] Yet these methods are also limited by their tedious procedures. It still remains a challenge to develop a simple and time-/energy-saving approach to synthesize HPCMs.

Herein, a simple and effective strategy is reported in preparing hierarchical porous carbon fibers (HPCFs) by using fibers of alginic acid, a non-toxic and biocompatible biomass. The obtained HPCFs exhibit a 3D network of nanosized carbon particles and a hierarchical porous architecture composed of both large mesopores (diameter ca. 19 nm) and abundant micropores (<2 nm). Whereas the large mesopores provide fast diffusion channels to ensure easy accessibility of electrolytes, the micropores shorten the Li diffusion distance thus decreasing the diffusion time. Due to the hierarchical porous structure and the stability of the 3D network, HPCFs show excellent rate capability and cycle stability when used as anode materials in LIBs. This paper provides insights into the potential applications of the alginate biomass-derived carbon materials for energy storage devices such as LIBs, which are characterized as sustainable development technology in views of the renewable and green raw materials and environmentally friendly process.[29,30]

Results and Discussion

Figure 1 shows typical scanning electron microscopy (SEM) and transmission electron microscopy (TEM) images along with an energy-dispersive X-ray (EDX) spectrum of as-prepared HPCFs. The regular and fiber-like shape of the alginic fibers was preserved after carbonizing (Figure 1 a). The filaments exhibit uniform one-dimensional morphology with a diameter of about 10 μm (Figure 1 b). EDX analysis (the inset in Figure 1 a) reveals that the HPCFs are mainly composed of carbon which accounts for 96.7 % in atomic ratio besides a small quantity of oxygen. Because alginic acid contains abundant carboxyl and hydroxy groups, the existence of oxygen may be ascribed to the remanent oxygen groups. The peaks of Pt in the EDX spectrum are from the ultrathin platinum coating layer deposited on the specimens before the SEM image. Figure 1 c shows the morphology of a single filament, which exhibits a smooth surface both on the exterior and cross section of the filament under low magnification. Under higher magnification (Figure 1 d), however, it is clear that the filament is composed of nanosized carbon particles (less than 10 nm) surrounded by fissures and hillocks to form a system of unhomogeneously porous structure. The typical TEM image (Figure 1 e) further proves that there are abundant interspaces around the nanoparticles, indicating that the obtained carbon fibers are composed of an interconnecting network of nanosized carbon particles and take on a hierarchical porous structure. Figure 1 f shows the typical HRTEM image of the as-prepared HPFCs. As can be seen, the carbon material exhibits a relatively disordered microstructure with curved and bent graphene sheets, indicating that the as-obtainted HPFCs are one kind of soft carbon.

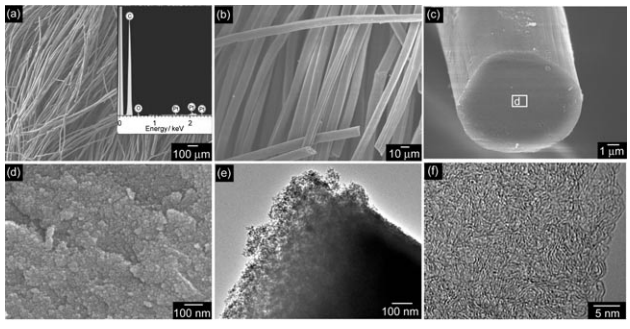

Figure 1. SEM (a, b, c, and d), EDX analysis (the inset in a), typical TEM (e) and HRTEM (f) images of the as-prepared HPCFs.

The nitrogen adsorption–desorption isotherms and corresponding pore size distribution curves by the density functional theory (DFT) method of the as-prepared HPCFs are shown in Figure 2. The obtained HPCFs exhibit a combined characteristic of type I/IV with Brunauer-Emmett-Teller (BET) surface area of 217 $m^2 g^{-1}$ (Figure 2 a). The adsorption below 0.1 increased steeply along with the relative pressure, indicating that there exist abundant micropores (<2 nm). The existence of hysteresis loop indicates the presence of mesopores. Obviously, there is a step emerging from the hysteresis loop at $P/P_0 = 0.5$, which may be related with a bimodal pore size distribution[31–33] in the sample. Usually, thermal treatment at high temperature is helpful for both the widening of micropores into mesopores and the formation of secondary mesoporous structures. Therefore, the stepped characteristic in the hysteresis loop may arise from the above mentioned two behaviors caused by calcination. The DFT pore-size distribution (Figure 2 b) indicates that the obtained HPCFs consist of abundant micropores with pore diameters ranging from 0.3 to 2 nm and varied mesopores (with diameter centered at about 19 nm) with a wide size distribution from 6 to 40 nm. As evidenced by SEM and TEM images, these pores are uniformly dispersed in the entire carbon fibers. After being filled with electrolyte during battery assembly, these hierarchical pores are expected to accelerate the transportation of Li^+ into the interior of carbon fibers.

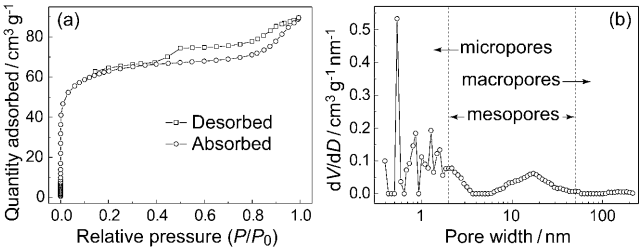

Figure 2. a) Nitrogen adsorption–desorption isotherms and b) the corresponding DFT pore size distributions of the as-obtained HPCFs.

Figure 3 a shows the Raman spectrum of the HPCFs. Two characteristic peaks at about 1337 and 1588 cm^{-1} correspond to the D-band and G-band of carbon, respectively. The D-band

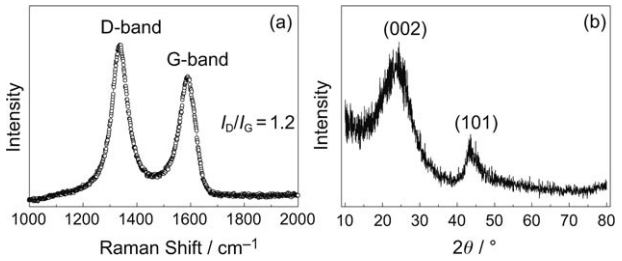

Figure 3. a) Raman spectrum and b) XRD pattern of HPCFs.

arises from an A_{1g} mode in the disordered region of carbon materials or edge plane of carbon powder, representing defects, curved graphite sheets, dislocations, and lattice distortions in carbon structures, whereas the G-band is engendered by an E_{2g} vibration mode in the graphitic region of carbon materials[34,35].

The ratio of the intensity of the D-band to that of the G-band ($R = I_D/I_G$) is 1.2, indicating the existence of a relatively large degree of disordered structure. The X-ray diffraction (XRD) pattern in Figure 3b reveals that two broad peaks appearing at $2\theta = 24.45^\circ$ and 43.56° correspond to the diffraction peaks of (002) and (101) planes of graphite structure, respectively. According to the Bragg's Law, the peak at $2\theta = 24.45^\circ$ corresponds to an interlayer distance (d_{002}) of 0.366 nm, whereas typically in a crystalline carbonaceous structure, such as graphite, the distance is 0.335 nm, indicating a low graphitization degree and a disordered interlayer structure of HPCFs.

The overall X-ray photoelectron spectroscopy (XPS) spectrum (Figure 4a) shows the existence of carbon (93.2%) and oxygen (6.8%), and this is consistent with the EDX result. In

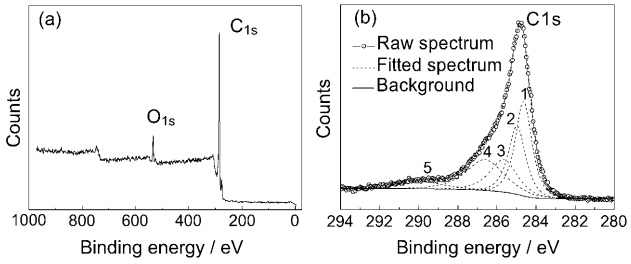

Figure 4. a) XPS survey spectrum and b) C1s spectrum of HPCFs.

order to obtain the quantitative information of oxygen-containing functional groups, the software package XPS Peak 3.1 was used to fit the high resolution C1s peak (Figure 4b). The results indicate that the C1s peak can be divided into five peaks centered at 284.5, 285.1, 286.2, 287.2, and 288.9 eV, respectively. Usually, the main peak at 284.5 eV originates from a graphite signal. The peak at 285.1 eV is attributed to sp^3-hybridized carbon atoms as those in diamond-like carbon. The peaks at 286.2, 287.2, and 288.9 eV correspond to hydroxyl, carbonyl (or ether), and carboxyl (or ester) groups, respectively.[36–40] These results indicate that the as-obtained HPCFs are enriched in oxygen-containing groups.

The structure characterizations indicate that the as-obtained HPCFs consist of 1D microscale carbon fibers, which are constructed by a 3D network of nanosized carbon particles and exhibit a hierarchical porous architecture. Due to the novel structure, the HPCFs are expected to exhibit superior electrochemical properties. Figure 5a shows the first five cyclic vol-

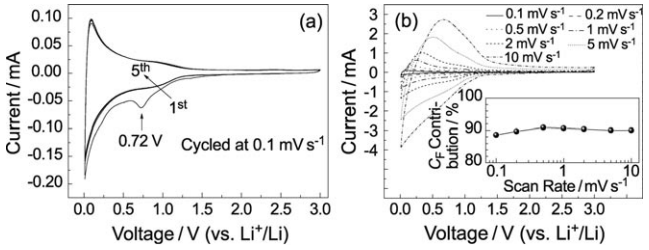

Figure 5. a) The first five CV curves cycled at 0.1 mV s^{-1}. b) Stable CV curves cycled at various scan rates from 0.1 to 10 mV s^{-1}.

tammograms (CV) curves for HPFCs electrode at a scan rate of 0.1 mV s^{-1} in the voltage window of 0.01–3.0 V (vs. Li$^+$/Li), which exhibits a typical CV behavior of carbon materials in lithium batteries.[17] Compared with the subsequent four cycles, an additional cathodic current peak appears approximately at 0.72 V (vs. Li$^+$/Li) in the first cycle, which could be ascribed to the decomposition of electrolyte. Furthermore, the reduction current in the first cycle below 1.8 V (vs. Li$^+$/Li) is obviously larger than that of the following ones. The extra current could be attributed to the formation of a solid electrolyte interphase (SEI) film, which results in the larger discharge capacity of the first cycle than that of the second cycle (Figure 6a). It should be noted that from the 2nd to the 5th cycles, the CV curves are almost overlapping with each other, which is consistent with the galvanostatic discharge/charge results, revealing the stability of the as-formed SEI film and a stable structure of the HPCFs. In Li-containing electrochemical systems, the total capacity is usually composed of the surface capacity due to non-faradic double layer capacitance and the faradic capacitance (C_F), relating to the Li$^+$ insertion process and the surface charge-transfer process. To determine the C_F contribution to the total capacity, we measured the CV patterns at various scan rates from 0.1 to 10 mV s^{-1} (Figure 5b). The value of C_F contribution is calculated based on the integral area of the

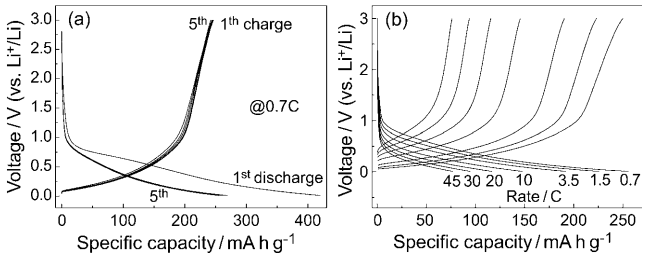

Figure 6. The galvanostatic discharge/charge curves of HPCFs for a) the initial five cycles at the rate of 0.7 C and b) rate capabilities at different current densities.

redox processes at lower voltage (Figure 5b inset). The C_F accounts for about 90% of the total capacity with little variation along with scan rates. These results indicate that the obtained HPCFs are promising electrode materials for high-power energy storage devices.

To demonstrate the potential application of HPCFs in anode materials for Li-ion batteries, we carried out a preliminary investigation into their electroactivity toward Li insertion-extraction. Figure 6a shows the discharge/charge curves of HPCFs in the initial five cycles at a rate of 0.7 C (completing the discharge or charge process in 85 min). The discharge plateau under 0.22 V, characteristic plateau of graphite structure, cannot be observed from the discharge curves, implying a low graphitization degree of HPCFs. This result is consistent with the Raman and XRD results. The voltage plateau at 0.8 V corresponds to the irreversible capacity due to the formation of the SEI that is common for carbon materials and consistent with the CV test. A discharge capacity of 420 mA h g^{-1} and a charge capacity of 255 mA h g^{-1} were observed in the first discharge/charge cycle, leading to an irreversible capacity of about 39%, which could be ascribed to the existence of oxygen-containing groups on the surface of HPCFs. Despite of the existence of irreversible capacity in the first cycle, from the 2nd to the 5th cycles, the discharge curves are almost overlapping with each other, revealing the excellent reversibility toward lithium insertion-extraction, which is also consistent with the CV results. No obvious voltage plateau is observed at lower voltage (below 0.01 V) in the discharge/charge curves of HPFCs at a rate of 0.7 C in the voltage range of −0.01–3 V and 0.0–3 V (vs. Li^+/Li) (not shown), indicating that the as-prepared carbon material is soft carbon which is consistent with the results from the HRTEM image (Figure 1f).

The as-prepared HPCFs also exhibit outstanding rate capabilities. When the current density is increased by about 30 times from 0.7 C to 20 C, the capacity retention of HPCFs can approach 50% (Figure 6b and 7a). Even at the very high rate of 45 C (completing the discharge or charge process within 80 s), a capacity of 79 mA h g^{-1} is still maintained. The capacity retention of HPCFs is much better than that of commercial graphite anode at higher rates (above 10 C). Figure 7a shows the comparison of high-rate capacity retention between HPCFs and commercial graphite cycled at various discharge/charge rates. Taking a high rate of 30 C for example, the capacity retention of HPCFs is about 40% of its capacity at 0.7 C, whereas that of graphite is only 8%. As far as carbonaceous materials are concerned, it is one of the best rate performances ever measured.[14,16–18]

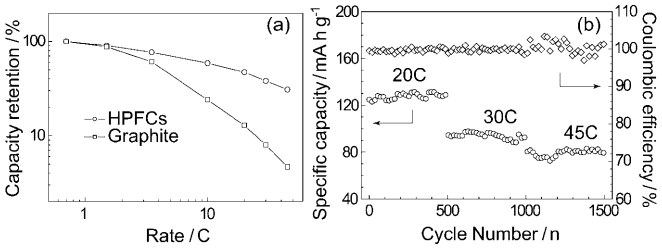

Figure 7. a) The capacity retention of HPCFs (circle) and commercial graphite (rectangle) at various rates; b) Cycling performance (circle) and the corresponding coulombic efficiency (diamond) of the HPCFs at rates of 20, 30, and 45 C in the voltage range of 0.01–3.0 V (vs. Li^+/Li).

In addition to the outstanding rate performance, the HPCFs also exhibit excellent cycle stability and high coulombic efficiency at high discharge/charge rates (Figure 7b). At 20 C, there is no obvious capacity fading even after 500 cycles. At the rate of up to 30 C and 45 C, the reversible capacity are 99.3% and 98.8% of the first cycle after 500 cycles (i.e., the capacity fading rate is only 0.0014% and 0.0024% per cycle, respectively).

The excellent electrochemical performances of the HPCFs can be attributed to their peculiar structures (i.e., the 1D micrometer-scale carbon fibers), which are constructed by a 3D network of nanometer-sized carbon particles and exhibit hierarchical porous architectures. Firstly, the nanometer-sized carbon particles in the 3D network of carbon matrix provide numerous active sites for Li^+ insertion/extraction reactions and the lithium ion diffusion length can be greatly decreased due to the small diameter of the carbon particles (less than 10 nm). Besides, high electrical conductivity can be achieved by the interconnected walls of the carbon particles. Secondly, the hierarchical porous architecture composed of both micropores and mesopores plays important roles in mass storage and migration. The function of the above two types of pores is similar to that of capillary vessels and arteries in human bodies. On the one hand, the abundant micropores can provide enough space for the electrolyte accommodation; on the other hand, the mesopores can provide expedite channels for liquid electrolyte transportation and lithium ion diffusion, making them easily arrive at the surface of the carbon particles. Finally, the existence of a 1D micrometer-scale nanostructure of carbon fibers guarantees good contact with electronically conductive carbon black when used as anode materials for LIBs, thus achieving a robust electronically conductive network of carbon materials.

Conclusions

1D HPCFs consisting of a 3D network of nanometer-sized carbon particles and a hierarchical porous architecture were successfully prepared by controlled carbonization of alginic acid fibers prepared through a simple wet spinning method. The nanometer-sized carbon particles of HPCFs were interconnected with each other, conceiving a 3D network of architecture. Varied mesopores and micropores with different shapes and sizes were formed around the nanoparticles, constructing a hierarchical porous network. The peculiar structure demonstrated that the HPCFs exhibit excellent rate capability and cycle stability. Our approach for the preparation of HPCFs from alginic acid with high Li-storage properties may open new prospects for utilization of biomass sources to produce high-performance anode materials for lithium-ion batteries.

Experimental Section

Preparation of hierarchical porous carbon fibers

Sodium alginate (Bright Moon Seaweed Group, Qingdao, 8 $ g^{-1}) was first dissolved in H_2O to form a homogenous solution and then extruded through spinneret holes into a coagulating bath containing hydrochloric acid solution, where an ion exchange reaction occurred between H^+ in the bath and Na^+ in the as-spun filament. Due to the insolubility of alginic acid in aqueous solution, alginic acid filaments would form. The wet alginic acid filaments were collected and washed with distilled water to remove adsorbent metal and chloride ions. After drying in air, the obtained alginic acid fibers were carbonized at 1500 °C in argon atmosphere for 6 h to yield HPCFs.

Structural characterization of HPCFs

TEM and SEM images of HPCFs were taken on a JEOL JEM-1011 electron microscope operated at 100 kV and a JEOL JSM-6700 F operated at 10 kV, respectively. The N_2 adsorption–desorption isotherms were recorded at 77.4 K on a Micromeritics ASAP 2020 system. Prior to the test, samples were vacuum dried at 473 K for 12 h to remove adsorbed guest species such as water. Pore size distribution was calculated through nonlocal DFT method. Raman spectrum was obtained on a Renishaw 1000 Raman spectrometer with the 514.5 nm excitation line of an Ar ion laser. XRD patterns were recorded on a Rigaku D-max-rA diffractometer with Cu-Kα radiation. XPS was performed on a VG Scientific ESCALab220i-XL XPS spectrometer.

Electrochemical characterization of HPCFs

Before conducting electrochemical tests, two-electrode Swagelok-type cells were assembled in an argon-filled glove box with metallic lithium foil as the counter electrode. To prepare the working electrodes, a mixture of active materials, super-P carbon and poly(-vinyl difluoride) (PVDF) was coated on a Cu foil in a weight ratio of 80:10:10. A glass fiber (GF/D) purchased from Whatman was used as separator. The electrolyte consisted of a solution of 1 M $LiPF_6$ in ethylene carbonate (EC)/dimethyl carbonate (DMC)/diethyl carbonate (DEC) (1:1:1, in wt%) (Tianjin Jinniu Power Sources Material Co., Ltd.). Galvanostatic cycling tests of assembled cells were carried out on an Arbin BT2000 system in the voltage range of 0.01–3.0 V (vs. Li^+/Li) at different current densities. Cyclic voltammograms (CVs) were performed on a Parstat 2273 advanced electrochemical workstation in the voltage range of 0.01–3.0 V (vs. Li^+/Li) with scan rates from 0.1 to 10 mV s^{-1}.

Acknowledgements

This work is supported by the National Natural Science Foundation of China (NSFC Nos. 50730005, 20821003, 20701038 and 50908120), Ministry of Science and Technology (MOST No. 2009CB930400), and the Knowledge Innovation Program of the Chinese Academy of Sciences (No. KJCX2-YW-W26).

Keywords: biomass · electrochemistry · lithium · mesoporous materials · microporous materials

[1] B. Hu, K. Wang, L. Wu, S.-H. Yu, M. Antonietti, M.-M. Titirici, *Adv. Mater.* **2010**, *22*, 813 – 828.
[2] S. H. Guo, J. H. Peng, W. Li, K. B. Yang, L. B. Zhang, S. M. Zhang, H. Y. Xia, *Appl. Surf. Sci.* **2009**, *255*, 8443 – 8449.
[3] F. Zhang, K. X. Wang, G. D. Li, J. S. Chen, *Electrochem. Commun.* **2009**, *11*, 130 – 133.
[4] W. Z. Shen, Z. F. Qin, H. G. Wang, Y. H. Liu, Q. J. Guo, Y. L. Zhang, *Colloids Surf. A* **2008**, *316*, 313 – 316.
[5] Y. Zhou, S. Kajiyama, K. Itoh, T. Tanino, N. Fukuda, T. Tanaka, A. Kondo, K. Fukui, *Appl. Microbiol. Biotechnol.* **2009**, *84*, 375 – 382.
[6] L. Sun, S. B. Zhou, W. J. Wang, X. H. Li, J. X. Wang, J. Weng, *Colloids Surf. A* **2009**, *345*, 173 – 181.
[7] Y. M. Qin, *Polym. Adv. Technol.* **2008**, *19*, 6 – 14.
[8] Y.-G. Guo, J.-S. Hu, L.- J. Wan, *Adv. Mater.* **2008**, *20*, 2878 – 2887.
[9] H. Li, Z. X. Wang, L. Q. Chen, X. J. Huang, *Adv. Mater.* **2009**, *21*, 4593 – 4607.
[10] P.-G. Bruce, B. Scrosati, J.- M. Tarascon, *Angew. Chem.* **2008**, *120*, 2972 – 2989; *Angew. Chem. Int. Ed.* **2008**, *47*, 2930 – 2946.
[11] J. Maier, *Nat. Mater.* **2005**, *4*, 805 – 815.
[12] M. Armand, J. M. Tarascon, *Nature* **2008**, *451*, 652 – 657.
[13] Y. P. Wu, E. Rahm, R. Holze, *J. Power Sources* **2003**, *114*, 228 – 236.
[14] C. Masarapu, V. Subramanian, H. Zhu, B. Wei, *Adv. Funct. Mater.* **2009**, *19*, 1008 – 1014.
[15] H. Q. Li, R. L. Liu, D. Y. Zhao, Y. Y. Xia, *Carbon* **2007**, *45*, 2628 – 2635.
[16] Y.-S. Hu, P. Adelhelm, B. M. Smarsly, S. Hore, M. Antonietti, J. Maier, *Adv. Funct. Mater.* **2007**, *17*, 1873 – 1878.
[17] X.-L. Wu, Q. Liu, Y.-G. Guo, W.-G. Song, *Electrochem. Commun.* **2009**, *11*, 1468 – 1471.
[18] V. Subramanian, H. Zhu, B. Wei, *J. Phys. Chem. B* **2006**, *110*, 7178 – 7183.
[19] Q. Wang, H. Li, L. Chen, X. Huang, *Carbon* **2001**, *39*, 2211 – 2214.
[20] A. M. Cao, J. S. Hu, H. P. Liang, W. G. Song, L. J. Wan, X. L. He, X. G. Gao, S. H. Xia, *J. Phys. Chem. B* **2006**, *110*, 15858 – 15863.
[21] H. P. Liang, N. S. Lawrence, L. J. Wan, L. Jiang, W. G. Song, T. G. J. Jones, *J. Phys. Chem. C* **2008**, *112*, 338 – 344.
[22] R. Gadiou, A. Didion, R. I. Gearba, D. A. Ivanov, I. Czekaj, R. Kotz, C. Vix-Guterl, *J. Phys. Chem. Solids* **2008**, *69*, 1808 – 1814.
[23] P. M. Barata-Rodrigues, T. J. Mays, G. D. Moggridge, *Carbon* **2003**, *41*, 2231 – 2246.
[24] J. Górka, M. Jaroniec, *J. Phys. Chem. C* **2008**, *112*, 11 657 – 11 660.
[25] C. F. Xue, B. Tu, D. Y. Zhao, *Adv. Funct. Mater.* **2008**, *18*, 3914 – 3921.
[26] M. Yang, G. Wang, *Colloids Surf. A* **2009**, *345*, 121 – 126.
[27] S. Sepehri, B. B. Garcia, Q. F. Zhang, G. Z. Cao, *Carbon* **2009**, *47*, 1436 – 1443.
[28] W. Xing, C. C. Huang, S. P. Zhuo, X. Yuan, G. Q. Wang, D. Hulicova-Jurcakova, Z. F. Yan, G. Q. Lu, *Carbon* **2009**, *47*, 1715 – 1722.
[29] H. Chen, M. Armand, G. Demailly, F. Dolhem, P. Poizot, J. M. Tarascon, *ChemSusChem* **2008**, *1*, 348 – 355.
[30] J.-M. Tarascon, *ChemSusChem* **2008**, *1*, 777 – 779.
[31] Z. B. Lei, Y. Xiao, L. Q. Dang, M. Lu, W. S. You, *Microporous Mesoporous Mater.* **2006**, *96*, 127 – 134.
[32] K. Nakagawa, S. R. Mukai, K. Tamura, H. Tamon, *Chem. Eng. Res. Des.* **2007**, *85*, 1331 – 1337.
[33] Suhas, P. J. M. Carrott, M. M. L. Ribeiro Carrott, *Carbon* **2009**, *47*, 1012 – 1017.
[34] S. Kawasaki, T. Hara, Y. Iwai, Y. Suzuki, *Mater. Lett.* **2008**, *62*, 2917 – 2920.
[35] H. P. Zhao, J. G. Ren, X. M. He, J. J. Li, C. Y. Jiang, C. R. Wan, *Electrochim. Acta* **2007**, *52*, 6006 – 6011.
[36] C. W. Huang, Y. T. Wu, C. C. Hu, Y. Y. Li, *J. Power Sources* **2007**, *172*, 460 – 467.
[37] S. H. Li, S. B. Zhang, X. H. Wang, *Langmuir* **2008**, *24*, 5585 – 5590.
[38] D. J. Malik, A. W. Trochimczuk, A. Jyo, W. Tylus, *Carbon* **2008**, *46*, 310 – 319.
[39] M. Sevilla, A. B. Fuertes, *Carbon* **2009**, *47*, 2281 – 2289.
[40] W. S. Tseng, C. Y. Tseng, C. T. Kuo, *Nanoscale Res. Lett.* **2009**, *4*, 234 – 239.

Received: February 11, 2010
Revised: March 9, 2010
Published online on May 17, 2010

